



## **Evaluation of different flow stress models for machining simulations of medium carbon steels**

Downloaded from: <https://research.chalmers.se>, 2026-04-16 05:31 UTC

Citation for the original published paper (version of record):

Ertürk, A., Malakizadi, A., Larsson, R. (2025). Evaluation of different flow stress models for machining simulations of medium carbon steels. *Procedia CIRP*, 133: 603-608.

<http://dx.doi.org/10.1016/j.procir.2025.02.103>

N.B. When citing this work, cite the original published paper.

20th CIRP Conference on Modeling of Machining Operations

# Evaluation of different flow stress models for machining simulations of medium carbon steels

Ahmet Semih Erturk<sup>\*,1</sup>, Amir Malakizadi<sup>1</sup>, Ragnar Larsson<sup>1</sup><sup>a</sup>*Division of Materials and Computational Mechanics, Department of Industrial and Materials Science, Chalmers University of Technology, Göteborg SE-41296, Sweden*<sup>b</sup>*Division of Materials and Manufacture, Department of Industrial and Materials Science, Chalmers University of Technology, Göteborg SE-41296, Sweden*\* Corresponding author. E-mail address: [erturk@chalmers.se](mailto:erturk@chalmers.se)

## Abstract

A reliable simulation of cutting forces and chip formation that requires only a few experiments for model calibration is crucial for cost-effective machinability assessment, cutting data optimization, and tool design. To achieve this goal, selecting a suitable flow stress model to represent the behavior of the workpiece material under extreme deformation conditions is the first step to establishing realistic machining simulations. This study demonstrates the applicability of an inverse approach for the parameter identification of phenomenological flow stress models with different levels of complexity, including the combined effects of strain, strain-rate and thermal softening/hardening. The 2D finite element simulations affirmed the capability of the presented approach for identifying the flow stress parameters regardless of the complexity of the implemented model. It is also observed that models with improved thermal softening and strain/strain-rate hardening terms provide better predictive capabilities for estimating the cutting forces and chip thickness in 2D, indicating an improvement between 7-15% compared to the Johnson-Cook model. However, the 3D finite element simulation of the cutting process using the calibrated models showed significantly larger deviations from the experimental measurements. An effort was made to explain the reasons for this discrepancy.

© 2025 The Authors. Published by Elsevier B.V.

This is an open access article under the CC BY-NC-ND license (<https://creativecommons.org/licenses/by-nc-nd/4.0>)

Peer-review under responsibility of the scientific committee of the 20th CIRP Conference on Modeling of Machining Operations in Mons

**Keywords:** Finite Element Method; Machining; Simulation; Turning

## 1. Introduction

Modeling and simulation of machining process is quite challenging due to the rapid and high-intensity deformation, resulting in very high values of strain, strain-rate and temperature. To develop material models that can simulate the material behavior under such extreme conditions, specific experimental and numerical approaches have been proposed in the literature based on either the Split Hopkinson Pressure Bar (SHPB) and Taylor's impact tests or the inverse modeling of the orthogonal cutting process. FE-based, semi-analytical and learning models and methods have been proposed in the literature [1, 2, 3] for the inverse identification of flow stress parameters using orthogonal cutting tests - proved to provide viable and efficient solutions with reasonable accuracy. Nevertheless, the selection of an appropriate material model itself plays a vital role in the

accuracy and reliability of the FE simulation results. This is because various material models offer different predictive capabilities to account for the material's strain, strain-rate and thermal hardening/softening behaviors, as explored in the literature [4, 5, 6]. For example, Calamaz et al. [5] implemented a modified Johnson-Cook (JC) model [4] for simulation of chip formation when machining Ti-6Al-4V. The model can account for the strain softening behavior at large ranges of deformation and it proved to provide a significant improvement over the original JC model in terms of chip morphology. Malakizadi et al. [6] also modified the JC model to include a more appropriate strain and thermal softening effects for 316L austenitic steel during machining. The predictions of forces and chip thickness improved significantly compared to the original JC. Aside from the JC model, the Zerilli-Armstrong (ZA) material model and its modifications are also widely used in the literature. For example, Jaspers and Dautzenberg [7] assessed the ability of JC and ZA models to represent the flow stress properties for AISI 1045 and AA6082-T6 using both high- and low-strain-rate

tests. Instead of the original model, Gurusamy and Rao [8] evaluated the capabilities of the modified ZA model to simulate the deformation behavior of Inconel 718 Ni-base superalloy. They investigated the flow stress predictions of the model based on a primary shear zone model and the SHPB tests, as well as the FE simulations of the orthogonal cutting test.

These investigations show the importance of selecting a suitable material model to represent the material's behavior during the machining process. To this end, this study examines the effectiveness of various flow stress models in capturing the intricate deformation behavior of a micro-alloyed carbon steel. The experimental data given in [9] suggest that carbon steels, in general, undergo a continuous thermal softening up to 400°C that follows a hardening response that is believed to be associated with dynamic strain aging (DSA): the interactions between mobile dislocations and solute atoms during material deformation [10]. The experimental data [11] also show that carbon steels soften with increasing deformation due to dynamic recovery and dynamic re-crystallization (DRX) processes. These showcase the inadequacy of the widely used JC model for modeling the flow stress properties of carbon steels under the range of strain, strain-rate and temperature common in metal cutting.

In this study, the JC model (here referred to as Model I) and two different models proposed by Childs [12] (Model II) and Malakizadi et al. [13] (Model III) are used to describe the flow stress property of the workpiece material. Additionally, a new modified JC model (Model IV) is presented that includes a more realistic representation of the thermal softening/hardening behavior for plain carbon steels. The performance of Models II, III and IV is evaluated in 2D and 3D cutting simulations, and the results are compared to those of the original JC model taken here as the reference. The model parameters are obtained using an inverse methodology incorporating the thermally enhanced distributed primary zone deformation (DPZD) model [2]. Optimal parameters are used in 2D simulations to compare with experimental data obtained by using the orthogonal cutting test. The parameters that give the closest predictions with respect to the corresponding experimental measurements are chosen to be used in 3D simulations. This allowed us to evaluate the performance of a given material model for machining simulations under both 2D and 3D conditions. Furthermore, the material parameters reported by Malakizadi et al. [14] for Model II were compared with those obtained in the current study to evaluate the robustness of the enhanced DPZD inverse approach.

## 2. Experimental details

Experiments are performed under dry cutting conditions on an EMCO 365 CNC lathe. Two setups are prepared for the experiments. In the first setup (i.e., O1-3), the Sandvik Coromant uncoated cemented carbide TCMW 16T304 H13A inserts without a chip breaker are used. The edge radii of the inserts are  $25\pm 3\mu\text{m}$ . The rake and clearance angles are  $0^\circ$  and  $7^\circ$ , respectively, when the inserts are mounted on the STGCR 2525M 16 holder. Before the experiment, the C38 steel (see [2] for chemical composition) cylindrical workpiece material, with a diameter of 158mm, was machined in the radial direction to create

2mm flanges to meet orthogonal cutting conditions during the experiment. The data collected from this setup is used to validate the results of 2D simulations. For the second setup (i.e., F1-4), the Sandvik Coromant uncoated cemented carbide CCMT 120404 PF inserts with chip breaker are used. The edge radii of the inserts are  $35\pm 3\mu\text{m}$ . The inserts are mounted on the holder SCLCR 2525M 12 which has  $95^\circ$  entering angle. The process in this setup is a face turning of a cylindrical workpiece, C38 steel, with a diameter of 158mm. This setup is used for validating the 3D simulations due to the inclusion of the detailed geometry of the insert and the effects of the chip breaker and the nose of the insert. The cutting conditions (i.e., cutting speed  $V_c$ , feed  $f$ , and depth of cut  $a_p$ ) for the experiments are given in Table 1.

Table 1. Cutting conditions for experiments

Test	Machining	$V_c$ (m/min)	$f$ (mm/rev)	$a_p$ (mm)
O1	Orthogonal	240	0.050	2
O2	Orthogonal	240	0.075	2
O3	Orthogonal	240	0.100	2
F1	Face turning	150	0.050	1
F2	Face turning	150	0.100	1
F3	Face turning	200	0.150	1
F4	Face turning	250	0.200	1

The cutting forces were measured using the Kistler 9257A three-component dynamometer. The average forces were reported for a short engagement time of about 5 seconds from the beginning of the cuts to avoid the influence of wear on the measured forces. The chips produced during face turning operations (F1-F4) were sampled, and their outer surfaces were examined using a LEO 1550 Gemini scanning electron microscope (SEM).

## 3. Material models

The investigated material models are presented in this section. In Table 2, the constitutive relations for the material models are given, while the parameters of the models and the calibrated values are stated in Table 3. In the constitutive relations,  $\sigma$ ,  $\epsilon$ ,  $\dot{\epsilon}$  and  $T$  are the stress, strain, strain-rate and temperature, respectively. Additionally,  $\dot{\epsilon}_{ref}$ ,  $T_{ref}$  and  $T_m$  represent the reference strain-rate, reference temperature, and melting temperature, respectively.

In Table 2, Model I is the commonly used JC flow stress model taken here as the reference material model to compare the other models with. Model II is the material model proposed by Childs in [12]. In this model, a complex thermal softening behavior is implemented which includes a thermal hardening behavior part as shown in Fig. 1. Aside from the thermal softening, this model also has a constant strain hardening after the strain limit  $\epsilon_c$  and a temperature effect on strain-rate hardening when the temperature is higher than the given limit of  $T_c$ . Model III is the flow stress model used by Malakizadi et al. in [13]. This model includes a different thermal softening behavior and also a combination of strain-rate hardening and thermal softening. The difference of the thermal softening behaviors of

Model I, II and III are shown in Fig. 1 with the data given in the literature for various carbon steels. It can be seen from Fig. 1 that Models I and III are not able to capture the thermal hardening behavior seen around 500-650°C. Lastly, Model IV is used for observing the effect of realistic thermal softening (including the thermal hardening part as in Fig. 1). Therefore, the thermal softening part of Model I is replaced by a more realistic one, as stated in Table 2 which is similar to the thermal softening part of Model II. It should be noted that the parameters of Model II are taken from [12] as  $a = 0.25$  and  $T_c = 600^\circ\text{C}$ . For Model IV, the parameters are determined as  $a = 0.2$ ,  $b = 25000$ , and  $T_{crit} = 700^\circ\text{C}$  based on the behavior of various steels in Fig. 1 where  $T_{crit}$  is the parameter associated with thermal hardening behavior.

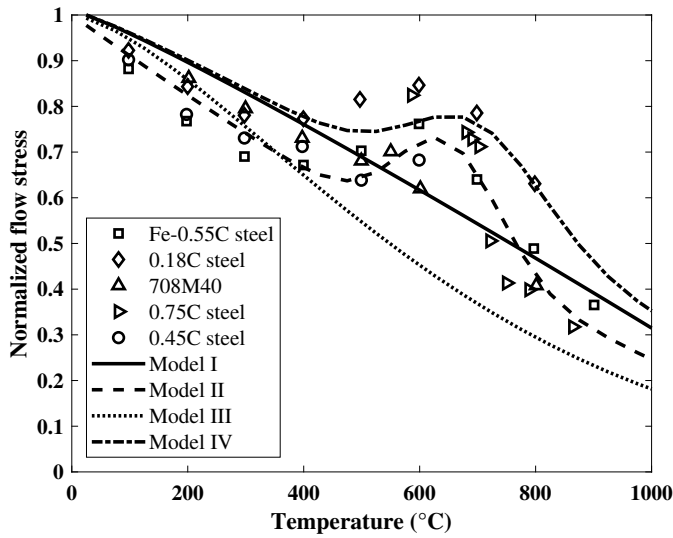


Fig. 1. Temperature dependent normalized flow stress presented by Model I, II, III and IV with the parameters given in Table 3 and the data given in [12] for various carbon steels.

The inverse identification process is performed with the cutting condition O2 (see Table 1) by using the enhanced DPZD inverse methodology [2]. It should be mentioned that the reason behind the selection of O2 is to make the calibration based on a mean cutting condition given that this condition has the mean feed among the orthogonal cutting tests. However, another identification method in [1] is also used for Model II to investigate the performance of the identification methods given in [1, 2], and the material model is called Model II\*. The identified parameters of the models are shown in Table 3.

#### 4. Simulation details

Cutting simulations are performed using the commercial software SFTC DEFORM 2D<sup>TM</sup> and 3D<sup>TM</sup>. The FE models are shown in Fig. 2. In 2D simulations, quadrilateral elements are used with a minimum element size of 0.005 mm. In the 3D simulations, the element type is tetrahedral, and the minimum element size is 0.02 mm. Forces and temperature are monitored until the simulations approach the steady state.

Table 2. Material Models and Constitutive Relations

Model No	Constitutive Relations
Model I	$\sigma = f(\epsilon) g(\dot{\epsilon}) h(T)$ $f(\epsilon) = A + B\epsilon^n$ $g(\dot{\epsilon}) = 1 + C \ln(\dot{\epsilon}/\dot{\epsilon}_{ref})$ $h(T) = 1 - [(T - T_{ref})/(T_m - T_{ref})]^m$
Model II	$\sigma = f(\epsilon) g(\dot{\epsilon}) h(T)$ $f(\epsilon) = \begin{cases} \sigma_0(1 + \epsilon/\epsilon_0)^n, & \epsilon \leq \epsilon_c \\ \sigma_0(1 + \epsilon_c/\epsilon_0)^n, & \epsilon \geq \epsilon_c \end{cases}$ $g(\dot{\epsilon}) = \begin{cases} (1 + \dot{\epsilon})^{m_0}, & T \leq T_c \\ (1 + \dot{\epsilon})^{m_0 + m_T(T - T_c)}, & T \geq T_c \end{cases}$ $h(T) = 1 - 0.00091T + 1.56 \times 10^{-7}T^2 \dots$ $\dots + a \exp[-6.5 \times 10^{-5}(T - 650)^2]$
Model III	$\sigma = f(\epsilon) g(\dot{\epsilon}, T)$ $f(\epsilon) = \lambda_1 + \lambda_2\epsilon^{\lambda_3}$ $g(\dot{\epsilon}, T) = \exp\left(-\left[1 - \lambda_4 \ln(\dot{\epsilon}/\dot{\epsilon}_{ref})\right]\left[\lambda_5 T/T_m\right]^{\lambda_6}\right)$
Model IV	$\sigma = f(\epsilon) g(\dot{\epsilon}) h(T)$ $f(\epsilon) = A + B\epsilon^n$ $g(\dot{\epsilon}) = 1 + C \ln(\dot{\epsilon}/\dot{\epsilon}_{ref})$ $h(T) = 1 - [(T - T_{ref})/(T_m - T_{ref})]^m \dots$ $\dots + a \exp[-(T - T_{crit})^2/b]$

Table 3. Identified material parameters based on the enhanced DPZD approach

Model (Calibrated Parameters)	Parameter values
Model I (A, B, n, C, m)	589, 146, 0.25, 0.069, 1.1
Model II ( $\sigma_0, \epsilon_0, n, m_0, m_T$ )	642, 0.01, 0.073, 0.0463, 0.0002
Model II* ( $\sigma_0, \epsilon_0, n, m_0, m_T$ )	480, 0.0055, 0.15, 0.035, 0.00012
Model III ( $\lambda_1, \lambda_2, \lambda_3, \lambda_4, \lambda_5, \lambda_6$ )	700, 367, 0.0884, 0.0814, 2, 1.5
Model IV (A, B, n, C, m)	589, 146, 0.25, 0.069, 1.1

\*Parameters are taken from [14]

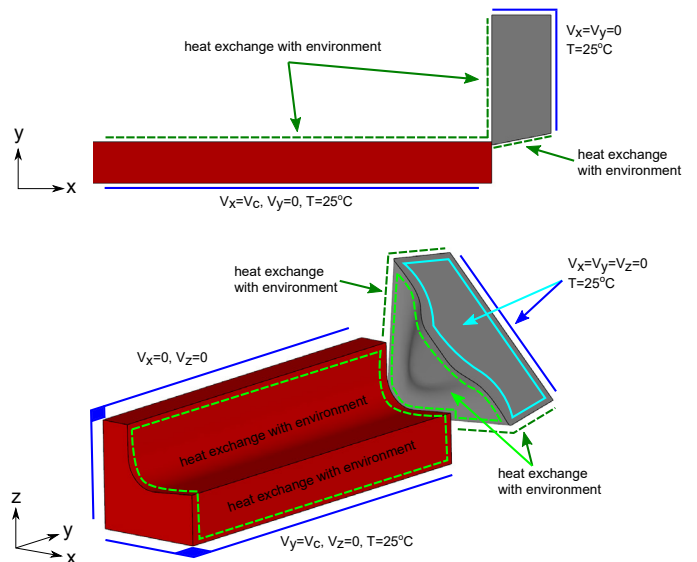


Fig. 2. Models and boundary conditions used in the simulations: 2D (top) and 3D (bottom)

In the simulations, the insert is assumed to be rigid, while the workpiece material is thermo-elastic-viscoplastic. The density, thermal conductivity and specific heat properties of the tool

and workpiece are taken from [2], while the elastic property of the workpiece material is obtained from JMatPro [15]. The heat transfer coefficient between the insert and the workpiece material is selected as  $10^5 \text{ kW/m}^2$ . For the friction, a pressure-dependent shear friction model is implemented as

$$\tau_f = \beta_1 k (1 - \exp(-\beta_2 P)) \quad (1)$$

where  $\beta_1$  and  $\beta_2$  are the model coefficients, while  $\tau_f$ ,  $k$  and  $P$  are shear stress, shear strength of the workpiece material and pressure at the interface, respectively. The parameters  $\beta_1$  and  $\beta_2$  are selected as 1 and 0.0045 based on [1, 2] in both 2D and 3D simulations.

## 5. Results and discussion

### 5.1. 2D simulation results

The performance of the models in 2D simulations is discussed based on the cutting conditions O1, O2, and O3 (see Section 2). The errors for the cutting force ( $F_c$ ), feed force ( $F_f$ ) and chip thickness ( $t_c$ ) are presented in Fig. 3. Considering the force errors for  $F_c$  and  $F_f$  in the figure, Model I leads to larger differences compared to other models. Model II, II\* and IV resulted in better predictions in terms of cutting force  $F_c$  and chip thickness  $t_c$ . Model III led to good estimations of the forces but poor estimations of the chip thickness. The total absolute error does not change much with increasing feed (i.e., from O1 to O3) when Model II and II\* are used for 2D cutting simulations. Models I and III gave a higher total absolute error for all presented cutting conditions. However, the performance of Model IV improved with increasing feed. Based on these, Model IV gives the overall best result followed by Model II and II\*.

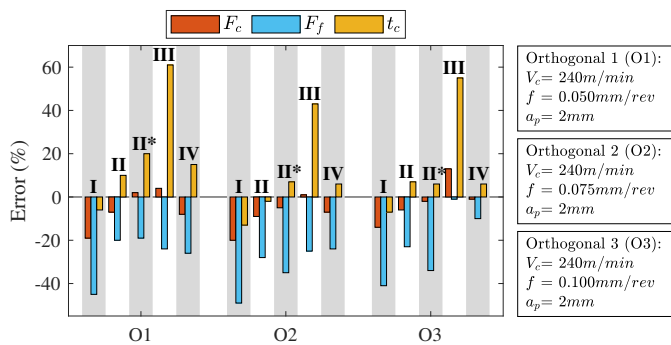


Fig. 3. Error between experiments and simulations for the 2D models.

When the simulation results of Models I and IV are compared, it is evident that the modifications made with respect to the thermal hardening term in Model I resulted in tangible improvements. This shows the importance of accurate temperature-dependent flow stress properties for cutting simulations, which is also noted in previous investigations [16]. To further justify whether this improvement is associated with the modification of the thermal softening/hardening term, the temperature distribution in the vicinity of the cutting edge at cutting condition O2 is presented in Fig. 4 for Model I. As evident,

the temperature at the tool-chip interface is around 600-700°C, which is within the temperature range where thermal hardening is expected for this material (see Fig. 1).

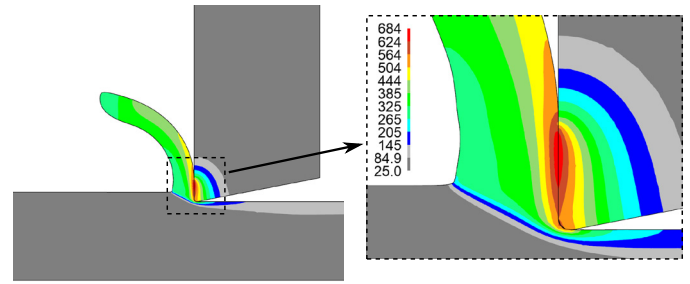


Fig. 4. Temperature (°C) distribution of 2D simulation of Model I (Johnson-Cook) for cutting condition O2

Moreover, by comparing Models II and II\*, the effect of the calibration method can be assessed. Based on the results, it is clear that both of the models yield overall good results. If we consider the absolute total error, Model II is a bit better than Model II\* for the stated cutting conditions. This shows the potential of the robust semi-analytical approach proposed by Erturk et al. [2] (used for Model II) for the calibration of material parameters of different material models. This calibration method is more efficient and requires only a few FE simulations, whereas a relatively larger number of FE simulations is required using the method proposed by Malakizadi et al. [1] (used for Model II\*). The latter inverse approach becomes even less efficient when the material model consists of a larger number of parameters. However, since the calibration is done based on FE simulations, it includes a known friction coefficient. For the method in [2], the friction coefficient is not included in the calibration method, so the friction coefficient must be determined separately.

### 5.2. 3D simulation results

Figure 5 shows the deviations in the cutting force ( $F_c$ ), the feed force ( $F_f$ ) and the passive force ( $F_p$ ) from the experimental measurements at cutting conditions F1-F4. The error in the estimated forces vary largely with the cutting condition and the implemented model. For example, even though the performances of Models I and IV are quite similar for cutting condition F1, they led to significantly different force estimations under cutting condition F2. However, it should be noted that the calculated absolute error for the estimated forces at these two cutting conditions is within the range of reported values in the literature for 3D cutting simulations [13]. As shown in Fig. 5, the results are largely overestimated for the other two cutting conditions (i.e., F3 and F4), especially the passive force overestimated by around 170%. Model II\* has the best overall performance, yet the total absolute error increases significantly with increasing cutting speed and feed (i.e., from F2 to F4). Comparing Models II and II\*, Model II\* yields better estimations for lower cutting speed and feed (F1 and F2) than Model II. However, the difference between the models is lower for higher cutting speed and feed (F3 and F4).

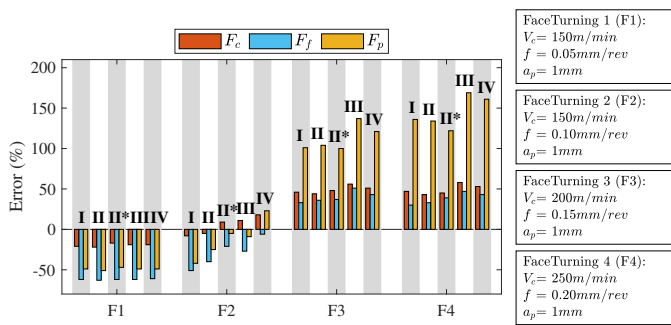


Fig. 5. Error between experiments and simulations for the 3D models.

The chip formation and the temperature distribution in the vicinity of the cutting edge at cutting condition F2 is presented in Fig. 6 for Model I. It can be seen that the temperature on the tool-chip interface is around 500-700°C which is within the temperature range where thermal hardening is expected (see Fig. 1). The maximum temperature for other models for the cutting condition F2 (i.e., around 660-740°C) is also within the range where thermal hardening is observed. However, the predicted maximum temperature is between 560-580°C when machining under cutting condition F1, which suggests that the temperature hardening behavior is not fully activated. This would explain the similarity in the force estimations at the cutting condition F1 in Fig. 5. Although the inclusion of thermal hardening behavior led to an overall improvement in force estimations in 2D simulations, such improvement was not evident in 3D simulation results - comparing the performance of Models I and IV for the cutting conditions F3 and F4 in Fig. 5.

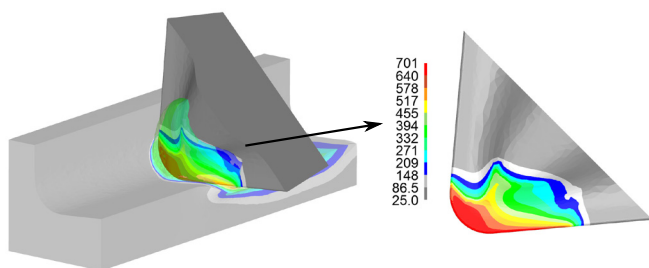


Fig. 6. Temperature (°C) distribution of 3D simulation of Model I (Johnson-Cook) for cutting condition F2

Such large deviations observed in the simulation results of the cutting conditions F3 and F4 could be associated with the exclusion of strain softening effect due to DRX or damage softening due to the formation of defects in the primary shear zone. The evaluation of the role of DRX requires a detailed investigation of chip cross-sections using advanced characterization methods and thus remains to be examined in the future. However, the analysis of the outer surfaces of the chips collected after machining under cutting conditions F1-F4 (see Fig. 7) already shows rather significant differences, which justifies the potential effect of damage softening. As shown in Fig. 7 (a1-d1), under the cutting conditions F3 and F4 with higher cutting speeds and feed rates, the chips are curled more profoundly and severely deformed as they are forced into the chip breaker ge-

ometry. Clearly, increasing the cutting speed and feed results in a more profound onset of serration during chip formation. Fig. 7(a2-d2) shows significantly shallower cracks on the outer surface of the chip under cutting condition F1 compared to those formed under cutting condition F4.

In general, the serration process originates from the intense local shear deformation due to severe thermal softening effect and/or crack formation due to the coalesce of micro-voids nucleated in the primary shear zones. These effects reduce the resistance of the material in front of the cutting edge at the primary shear zone and thus decrease the forces  $F_c$ ,  $F_f$  and  $F_p$ . Since these effects are not included in 3D FE simulations, a large overestimation in forces is observed between the simulated and experimental results under the cutting conditions F3 and F4. As a reference regarding this aspect, the study by Vilumsen and Fauerholdt [17] can be looked into, which shows the significance of the effective plastic failure strain (PSFAIL) in 3D cutting simulations. Moreover, some of the deviations in the 3D simulations could be related to frictional conditions. As mentioned in Section 2, two different setups are used for the experiments. The tools in the setups have different compositions (and supposedly different surface topographies). These can have some impact on the tribological conditions at the tool-chip interface, influencing frictional forces [18].

The other reason for observing markedly different predictive capabilities in 2D and 3D simulations may stem from the differences in element type, element density and time incrementation. The element types in 2D and 3D simulations are different (quadratic vs. tetrahedron), which can change the results due to different element formulations. Likewise, element size in the simulations in 2D and 3D creates differences to some extent, which is important when it comes to capturing a good resolution in the structure. By using smaller elements, the effects resulting from interpolations in the elements can be reduced, thus increasing the accuracy of the simulations. However, the downside is the significantly longer computational time. Additionally, selecting very small elements for the simulations may cause concentrated high deformation resulting in high strain and high strain-rates in the elements. This may deviate from the results and affect the accuracy negatively. Moreover, the time increments required to obtain convergence in the simulations are different. Smaller time increments are required for 3D compared to 2D. This is perhaps due to the non-linearity associated with different FE formulations as well as the dimension.

## 6. Conclusion

In conclusion, the performance of four different flow stress models has been investigated for the simulation of metal cutting processes. This study underscores the importance of the realistic representation of material behavior to obtain reliable predictions in cutting simulations - particularly in the case of 3D simulations. It was shown that including the effect of temperature on strain-rate hardening and assuming that strain hardening was constant after a critical strain value due to dynamic recovery (as in Model II) led to a better representation of the material behavior. Thus, Model II appears to be the most suitable flow stress

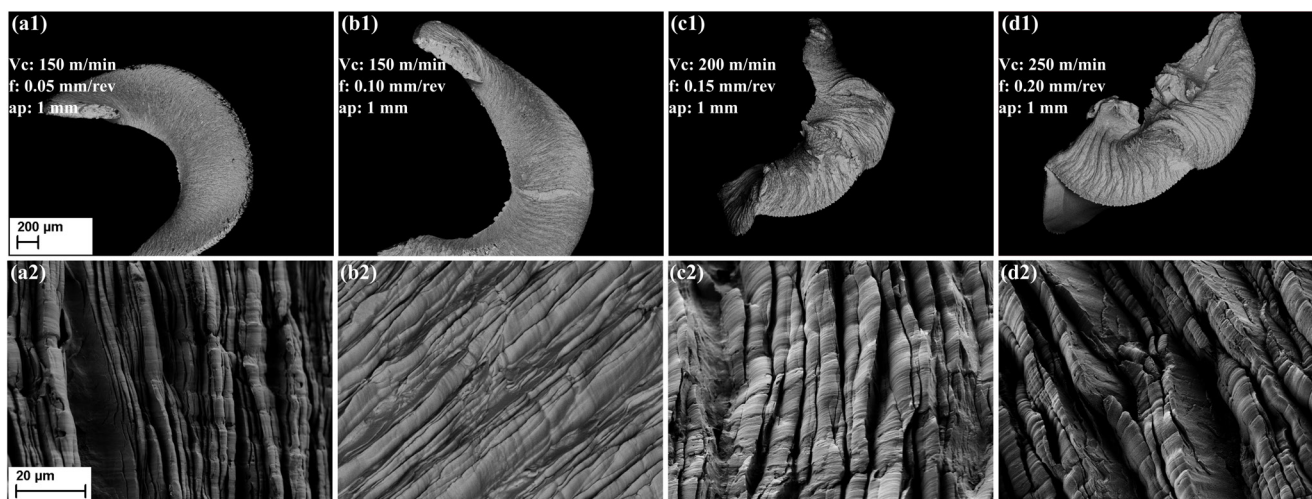


Fig. 7. SEM Chip images from experiments F1 (a), F2 (b), F3 (c) and F4 (d)

model for the metal cutting simulations of C38 steel among the investigated models. Comparing the overall performance (2D and 3D) of Model II and II\* suggested that the material parameters obtained using different calibration methods did not lead to significant differences in prediction results. This showed that the enhanced DPZD inverse methodology can offer a robust and efficient approach for the calibration of an arbitrary material model without the need for executing many costly FE simulations. The models are less predictive for cutting conditions with a higher cutting speed and feed in 3D. This demonstrates that, in addition to the critical role of the flow stress, the adoption of an appropriate damage/failure model is essential for accurate 3D cutting simulations.

## Acknowledgements

This research was financially supported by the Swedish national research program Vinnova-FFI, project no. 2016-05397.

## References

- [1] Amir Malakizadi, Stefan Cedergren, Ibrahim Sadik, and Lars Nyborg. Inverse identification of flow stress in metal cutting process using Response Surface Methodology. *Simulation Modelling Practice and Theory*, 60:40–53, 2016.
- [2] Ahmet Semih Erturk, Amir Malakizadi, and Ragnar Larsson. A thermo-mechanically motivated approach for identification of flow stress properties in metal cutting. *International Journal of Advanced Manufacturing Technology*, 111(3-4):1055–1068, 2020.
- [3] F. Ducobu, N. Kugalur-Palanisamy, G. Briffoteaux, M. Gobert, D. Tuytens, P. J. Arrazola, and E. Rivi'ere-Lorph'evre. Identification of the constitutive and friction models parameters via a multiobjective surrogate-assisted algorithm for the modeling of machining— application to arbitrary lagrangian eulerian orthogonal cutting of ti6al4v. *Journal of Manufacturing Science and Engineering*, 146(6):061005, 04 2024.
- [4] G. R. Johnson and W. Cook. A constitutive model and data for metals subjected to large strains, high strain rates and high temperatures. In *Proc. 7th International Symposium on Ballistics*, pages 541–547, 1983.
- [5] Madalina Calamaz, Dominique Coupard, and Franck Girot. A new material model for 2D numerical simulation of serrated chip formation when machining titanium alloy Ti–6Al–4V. *International Journal of Machine Tools and Manufacture*, 48(3-4):275–288, 2008.
- [6] Amir Malakizadi, Jannick Nils Oberbeck, Martin Magnevall, and Peter Krajnik. A new constitutive model for cutting simulation of 316L austenitic stainless steel. *Procedia CIRP*, 82:53–58, 2019.
- [7] S. P.F.C. Jaspers and J. H. Dautzenberg. Material behaviour in conditions similar to metal cutting: flow stress in the primary shear zone. *Journal of Materials Processing Technology*, 122(2-3):322–330, 2002.
- [8] Murali Mohan Gurusamy and Balkrishna C. Rao. On the performance of modified Zerilli-Armstrong constitutive model in simulating the metal-cutting process. *Journal of Manufacturing Processes*, 28:253–265, 2017.
- [9] T Shirakashi, K Maekawa, and E Usui. Flow stress of low carbon steel at high temperature and strain rate. I: Propriety of incremental strain method in impact compression test with rapid heating and cooling systems. *Bulletin of the Japan Society of Precision Engineering*, 17(3), 1983.
- [10] J. M. Robinson and M. P. Shaw. Microstructural and mechanical influences on dynamic strain aging phenomena. *International Materials Reviews*, 39(3):113–122, 1994.
- [11] Joshua Priest, Hassan Ghadbeigi, Sabino Ayvar-Soberanis, Anders Liljerehn, and Matthew Way. A modified Johnson-Cook constitutive model for improved thermal softening prediction of machining simulations in C45 steel. *Procedia CIRP*, 108(C):106–111, jan 2022.
- [12] Thomas H C Childs. Revisiting flow stress modelling for simulating chip formation of carbon and low alloy steels. *Procedia CIRP*, 82:26–31, 2019.
- [13] Amir Malakizadi, Hans Gruber, Ibrahim Sadik, and Lars Nyborg. An FEM-based approach for tool wear estimation in machining. *Wear*, 368-369:10–24, 2016.
- [14] Amir Malakizadi, Bin Shi, Philipp Hoier, Helmi Attia, and Peter Krajnik. Physics-based approach for predicting dissolution–diffusion tool wear in machining. *CIRP Annals*, 69(1):81–84, 2020.
- [15] Z Guo, N Saunders, J P Schill'e, and A P Miodownik. Material properties for process simulation. *Materials Science and Engineering: A*, 499(1-2):7–13, 2009.
- [16] Friedrich Bleicher, Christian Baumann, Stephan Krall, Steven P. Mates, Sibylle Herzig, Tim Alder, and Norman Herzig. Considering the influence of heating rate, complex hardening and dynamic strain aging in aisi 1045 machining: experiments and simulations. *CIRP Annals*, 70(1):49–52, 2021.
- [17] Morten F Villumsen and Torben G Fauerholdt. Prediction of cutting forces in metal cutting, using the finite element method, a lagrangian approach. In *Proceedings of the 7th German LS-DYNA Forum*, volume 8, 2008.
- [18] M. Fallqvist, F. Schultheiss, R. M'Saoubi, M. Olsson, and J. E. Ståhl. Influence of the tool surface micro topography on the tribological characteristics in metal cutting: Part I experimental observations of contact conditions. *Wear*, 298-299(1):87–98, 2013.